Growth modes of nanocrystalline Ni/Pt multilayers with deposition temperature

ARTICLE *in* JOURNAL OF APPLIED PHYSICS · AUGUST 2007

Impact Factor: 2.18 · DOI: 10.1063/1.2769785

Growth modes of nanocrystalline Ni/Pt multilayers with deposition temperature

V. Karoutsos,[a] P. Papasotiriou, and P. Poulopoulos
Materials Science Department, University of Patras, 26504 Patras, Greece

V. Kapaklis and C. Politis[b]
School of Engineering, Engineering Science Department, University of Patras, 26500 Patras, Greece

M. Angelakeris, Th. Kehagias, and N. K. Flevaris
Department of Physics, Aristotle University of Thessaloniki, 54124 Thessaloniki, Greece

E. Th. Papaioannou
Institut für Experimentalphysik, Freie Universität Berlin, Arnimallee 14, D-14195 Berlin-Dahlem, Germany

(Received 7 May 2007; accepted 29 June 2007; published online 29 August 2007)

We compare the structure and growth modes of two series of nanocrystalline Ni/Pt multilayers deposited on glass, Si, and polyimide substrates by electron-beam evaporation at room temperature (40 °C) and at 200 °C. X-ray diffraction patterns are recorded in order of the quality of the layering to be examined. The morphology of the films is studied by atomic force microscopy. The roughness of the samples is found to depend on the substrate and the total thickness, following a power law. The crystal structure, the shape of the crystallites, and the layering of the samples were determined by transmission electron microscopy. Differences in the shape of the crystallites and the surface morphology between the two series of samples are observed and they are understood within the framework of structural zone models. Finally, it is demonstrated the large stability of the multilayer structure for a period of at least 12 years. © *2007 American Institute of Physics*.
[DOI: 10.1063/1.2769785]

I. INTRODUCTION

Ni/Pt compositionally modulated multilayers have recently attracted some attention due to their interesting magnetic and magneto-optical properties, see, for example, Refs. 1–4. This system exhibits perpendicular magnetic anisotropy for thin Ni layers and for thicker ones, provided that they are separated by very thin Pt layers.[2] The magneto-optic properties show enhancement at the higher energy part of the Kerr rotation spectrum, above 3 eV.[2,4] These features render Ni/Pt multilayers an interesting system for magnetic and magneto-optic recording. Ni/Pt multilayers have also been used as a prototype system to study spin and orbital magnetic moments and to deduce, by theory and experiment, the layer-resolved magnetic moment profile for the full multilayer period.[5–7] A previous study has dealt with structural properties of Ni/Pt multilayers grown mainly at elevated temperatures (about 200 °C) on glass, Si, and polyimide substrates.[2] Growth at elevated temperatures reinforces perpendicular magnetic anisotropy.[8] Recently, magnetic and magneto-optic features useful for applications have also been reported for a series of samples grown at room temperature (40 °C).[4]

In the present work, we mainly focus on the growth of Ni/Pt multilayers at 40 °C on similar substrates and the outcome is compared to the result for the 200 °C series. It is found that the 40 °C growth results in the formation of smaller crystallites with a narrow size distribution following a logarithmic-normal (lognormal) behavior. Narrow-size distribution of grains is important for the development of future magnetic recording media where one seeks even for monodisperse nanostructures.[9] The surface roughness is seen to originate from grain boundary formation. For films of constant thickness, surface roughness is found to depend on the kind of substrate, being maximum for polyimide, small for glass, and even smaller for Si. The surface roughness increases with thickness following a power law behavior. The layering inside the grains is regular and it is almost of the same quality as for samples grown at higher temperatures. Samples grown at 200 °C consist of columnar (cylindrical-like) crystallites with a broad diameter-size distribution. Samples grown at 40 °C show a large fraction of spherical-like crystallites. Due to the lower deposition temperatures the columns are as small as the spheres in diameter. These results may be well-understood within the structural zone models at the transition area between zones I and II, taking into account the different ratios of T_S/T_m, where T_S is the substrate temperature and T_m the melting point of the samples.[10] Finally, it is demonstrated the long-term stability of the multilayer sequence over a period of at least 12 years. This observation is important for the applications of Ni/Pt multilayers as magnetic or magneto-optic recording media, indicating that hard disks made out of Ni/Pt multilayers will be stable for at least 12 years.

II. EXPERIMENTAL DETAILS

Ni_n/Pt_m multilayers were grown on glass, Si, and polyimide (Kapton) substrates by electron (e)-beam evaporation

[a]Author to whom correspondence should be addressed; electronic mail: vkar@upatras.gr
[b]Also at: Forschungszentrum Karlsruhe, Institut für Nanotechnologie, P.O. Box 3640, 76021 Karlsruhe, Germany.

in a chamber with base pressure of about 5×10^{-9} mbar. (The indices denote numbers of atomic planes in the multilayer period.) The deposition rates were kept constant at about 0.1 nm/s via a quartz balance system with feedback to the power supplies of the electron guns. The deposition temperature T_S was maintained at 40 °C. In the beginning of each evaporation a 20 nm buffer layer of Pt was grown in order to isolate the multilayer from the substrate and to allow for better crystallinity and {111} texturing. The multilayer growth was always ending at a 3–5 nm capping Pt layer for chemical protection of the samples against oxidation and corrosion.

The film morphology was revealed by atomic force microscopy (AFM) images recorded via a multimode scanning probe microscope (Digital Instruments). We have used AFM contact mode with the constant force method (the force between the sample surface and the AFM tip was kept constant by a feedback system while the surface beneath the tip was scanned). We have used a standard 15 μm$\times$15 μm piezoscanner with vertical range 2.5 μm and z-axis resolution 0.05 nm. The scan rate was 2 Hz. The cantilevers were V shaped with spring constants 0.06 and 0.12 N/m. The shape of the silicon nitride tips was square pyramidal with radius of curvature ~20 nm and half angle 35°. The images were processed with a linear plane fit in order to remove any sample tilt on them.

The software accompanying the multimode scanning probe microscope has rather limited capabilities. We have therefore developed a special program, which is able to process an AFM image data file in order to compute several physical quantities concerning the whole sample or a user-defined part of it. The program is also able to produce density and surface plots by using the well-known "gnuplot" package internally. Our program is written in FORTRAN 95.

The structural characterization was mainly performed with the help of x-ray diffraction (XRD) patterns recorded using a standard powder diffractometer (SEIFFERT) with Co- and Ni-filtered Cu Ka_1 radiation ($\lambda=0.154\ 059$ nm). Selected samples for cross-section transmission electron microscopy (XTEM) investigation were prepared by the sandwich technique, followed by the standard mechanical thinning and ion milling processes to reach electron transparency. TEM observations were performed in a 200 kV Jeol 2011 (0.19 nm point resolution, Cs=0.5 mm) electron microscope.

Finally, polar Kerr rotation was recorded with the help of a simple cross-polarizer-based experimental setup operating with a red He-Ne laser and Si-photodiode detection. The maximum field, applied along the normal-to-the sample surface direction, was 320 kA/m.

III. RESULTS

A. Layering

$\theta-2\theta$ XRD patterns have enabled us to revealed (i) the face centered cubic (fcc) structure of the multilayers, (ii) the existence of {111} texture, (iii) the quality of the multilayer stacking, and (iv) the average size of the crystallites. In Fig. 1 one may see the high-angle XRD pattern recorded on a

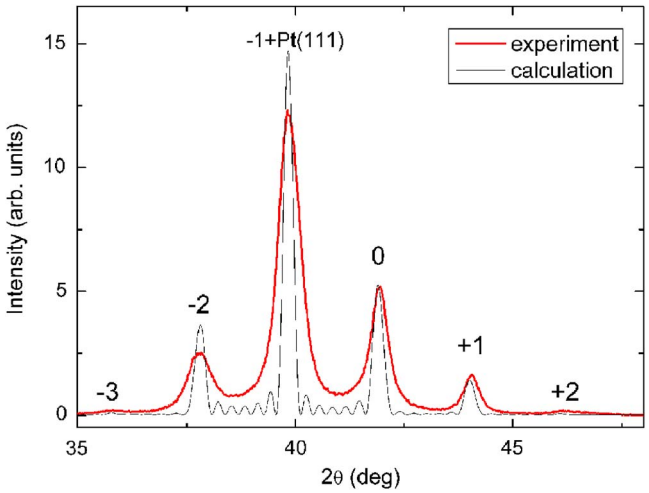

FIG. 1. (Color online) Experimental (thick) and calculated (thin line) high-angle x-ray diffraction pattern for a Ni_{10}/Pt_{11} multilayer grown on Si(111).

Ni_{10}/Pt_{11} multilayer grown on a silicon(111) substrate. The number N of multilayer periods was equal to 40. A solid solution peak (labeled as "0") is surrounded by many satellites of negative or positive order as indicated. The solid solution peak originates from Bragg's law for the average interplanar spacing in the multilayer (see also the discussion on the XTEM result in the next section) and allows for the determination of the stoichiometry of the multilayer with the help of Vegard's law.[11] The appearance of satellites is the result of interference effects. One has to think that the multilayer is actually an interference grating for x rays, since the multilayer period is comparable to the wavelength of x rays: the better the quality of the interfaces, the higher the intensity of the satellites. In Fig. 1 we have also included the calculated pattern for an ideal Ni_{10}/Pt_{11} multilayer, i.e., one with perfect interfaces free from interdiffusion or roughness. The calculations have been made within the model analyzed in Ref. 2. The coincidence at the position of the diffraction peaks between the experimental and the calculated pattern proves that the stoichiometry was correctly determined. On the other hand, one may see that the relative intensities of the satellites "−1" to "−3" are slightly smaller in the experimental pattern, as evidence that there is some roughness and/or interdiffusion at the interface.

In order to better check for the quality of the interfaces one has to characterize multilayers with short period. For example, it was shown that multilayers grown at 200 °C are almost perfect, while interdiffusion is present only at the monolayer limit.[6] In Fig. 2 we show the experimental and the calculated high-angle XRD pattern of a Ni_5/Pt_5 multilayer with $N=30$ grown on silicon (the best fitting, as far as concerns the peak positions, was received for $n=4.7$ and $m=5.3$). One may observe that the relative ratio of the satellite −1 between the experimental and the calculated pattern is quite different. The decrease of the experimental satellite peaks as compared to the calculated ones indicates the degradation of the interface quality. However, one has to think that as compared to the Ni_{10}/Pt_{11} multilayer, the Ni_5/Pt_5 multilayer has about two times more interfaces for the same length due to its much shorter period and, consequently, the

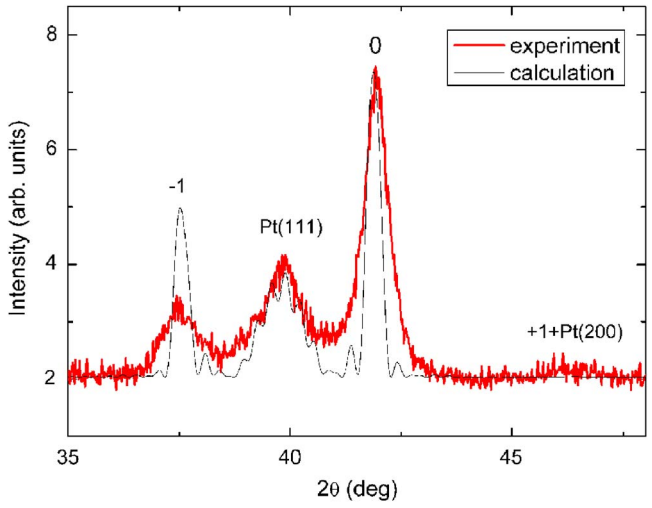

FIG. 2. (Color online) Experimental (thick) and calculated (thin line) high-angle x-ray diffraction pattern for a Ni_5/Pt_5 multilayer grown on Si(111).

interface effects are more prominent. It is very encouraging the fact that for a multilayer with only about five monolayers of each constituent in the multilayer period one may clearly observe satellite diffractions.

In Ref. 2 a mathematical tool was developed to characterize the quality of the multilayer stacking via the determination of a quality factor Q. $Q=100\%$ indicates a multilayer with ideal rectangular composition profile, i.e., one with ideal interfaces.[2] If one applies this model to the two samples of Figs 1 and 2, one deduces $Q=87.4\%$ and $Q=57.7\%$, respectively. Direct comparison to values of Q determined for multilayers with similar values of n, m evaporated at higher temperatures,[2] shows that when n and m are large enough, the quality factors do not depend on the substrate temperature. However, for small values of n and m multilayers grown at higher substrate temperatures have larger Q values of about 70%–80%. The substrate temperature of 200 °C does not promote interdiffusion beyond the first atomic layer at the interface.[6,7] Obviously, the lower substrate temperature of 40 °C, used in this study, cannot be responsible for a larger effect of interdiffusion. Consequently, the additional decrease of Q values for the series of the multilayers grown at 40 °C may be interpreted as an indication of larger roughness at the Ni/Pt interface, as compared to samples grown at 200 °C. This may be understood in terms of lower diffusivity of the adatoms impinging on the substrate due to the decreased substrate temperature.[10,11] This conclusion is also supported by the XTEM data discussed in the next section.

B. Crystal growth and surface roughening

In Fig. 3 one may see AFM images and grain-size distributions for a series of Ni/Pt multilayers of different thickness t, (a) 85, (b) 108, (c) 138, and (d) 206 nm. The n, m values of the multilayers are shown in Table I. Figure 3 reveals that our samples consist of grains with a homogeneous size distribution. In order to obtain the grain-size distribution, grain size measurements were made based on the AFM images. The average value of the largest and the least linear distance of the grains in a photograph was regarded as the diameter and was manually measured using the image software package SigmaScan Pro 5. In order to get good statistics, at least 400 grains were measured per image.

The histogram grain-size distribution is shown in Fig. 3. The line is the best-fitted lognormal function[12]

$$f(D)=\frac{k}{\sigma\sqrt{2\pi}}\exp\left[-\frac{(\ln D-\ln D_G)^2}{2\sigma^2}\right], \tag{1}$$

where the three fitting parameters are D_G, equals the mean grain size, σ is the standard deviation of $\ln D$, and k is a normalization constant. For all samples the fitted lognormal distribution is in good agreement with the histogram distribution in the whole grain-size range. The mean grain size (D_G) and standard deviation (σ) determined from this method are presented in Table I. The results for the mean grain size are in very good agreement (usually better than 10%) with the corresponding values obtained with the help of the Scherrer formula and input the full width at half maximum ($FWHM_{2\theta}$) of the solid solution diffraction peaks in the high-angle XRD patterns of the multilayers.[13] A detailed discussion on the equivalence and the limitations of the two methods, based on AFM and XRD measurements, for the determination of the mean grain size of metallic thin films is provided recently in Ref. 14.

The mean grain size for the samples grown on glass, was found to increase from 21.65 to 32.01 nm when the thickness of the samples increase from 85 to 206 nm (Table I). In Fig. 4(a) we display a plot of $\log(D_G)$ as a function of $\log(t)$. The error bars on the curve give the standard deviation of the values. For this region of thickness the relation between D_G and t seems to follow a power law of the form D_G-t^n. Linear regression results in $n=0.45\pm0.06$. Similar behavior has been recently observed in other metallic films, see, for example, Refs. 15 and 16. Various studies have shown that in metallic thin films there is a linear relationship between grain size and thickness of the film only for thickness less than a particular value. For thickness higher than this value the mean grain size remains practically constant.[17–19] Thus, we suggest that our plot depicts the region where the grain size increases linearly with thickness.

Analysis of the AFM data allows for quantitative information on the surface roughness. Root-mean-square roughness, R_{rms}, which is defined as the standard deviation of the surface height profile from the mean height, is the most commonly reported measurement of surface roughness and is given by

$$R_{rms}=\left[\frac{1}{N}\sum_{i=1}^{N}(z_i-\langle z\rangle)^2\right]^{1/2}, \tag{2}$$

where N is the number of pixels in the image (or data points), z_i is the height of the ith pixel, and $\langle z\rangle$ is the mean height of the image. The AFM software program evaluates the z_i for every (x_i,y_i) point of the image, so that $\langle z\rangle=0$. R_{rms} values given in Table I are the average values of at least five different regions for each sample. The size of each region is 1×1 μm^2. Within the accuracy of the measurement, which depends on the finite tip radius (this is because the AFM image represents not the shape of the surface itself but some

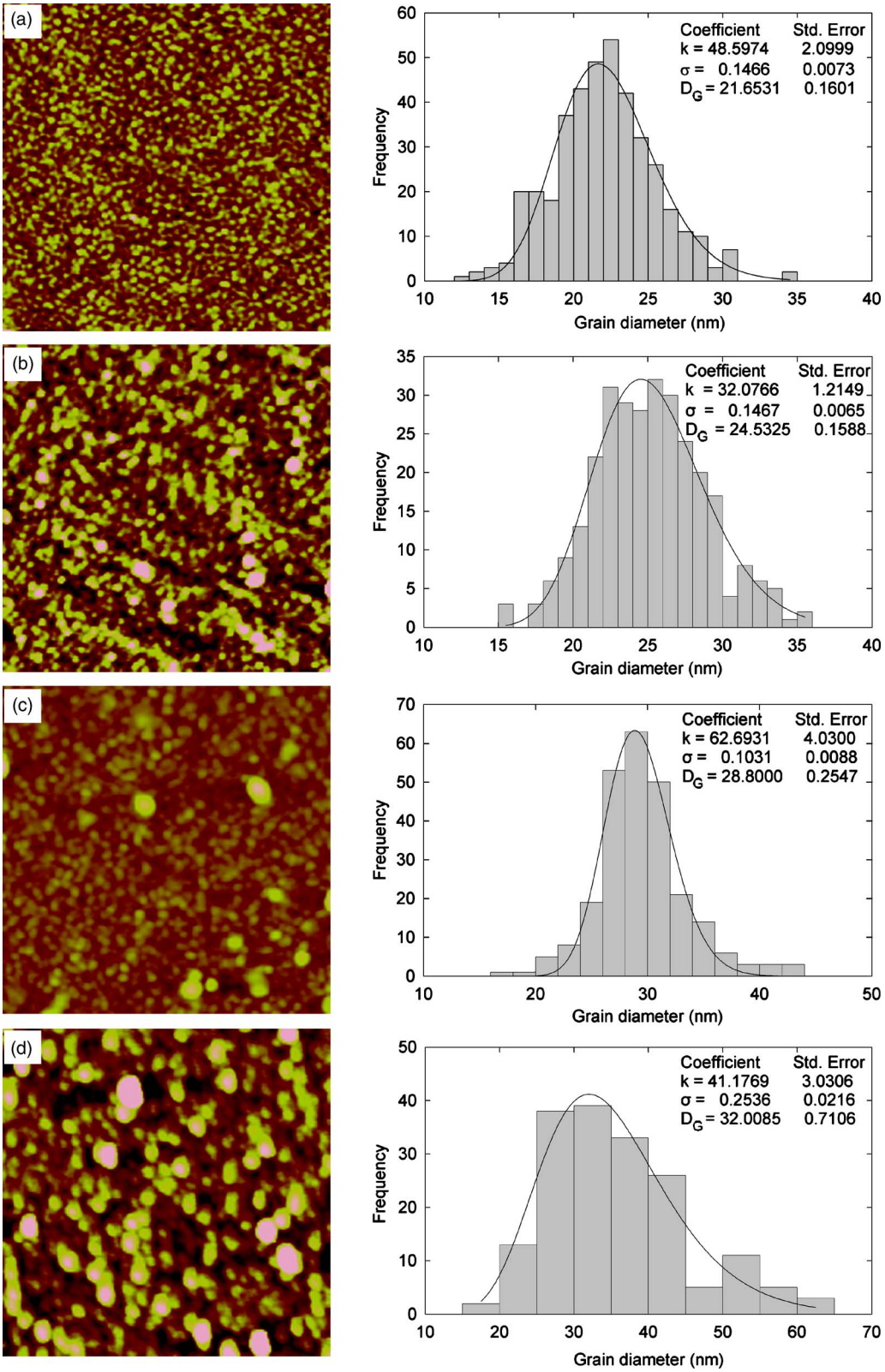

FIG. 3. (Color online) AFM images and grain-size distributions for nanocrystalline Ni/Pt multilayers grown on glass at different thickness: (a) 85, (b) 108, (c)138, and (d) 206 nm. The size of the images is 1×1 μm^2.

convolution of the surface and tip shapes), we evaluated the average roughness values for the four samples grown on glass (Table I) and we plotted them as a function of thickness t in Fig. 4(b). The bars on the curve give the error of the R_{rms}, which is $\delta R_{rms}=(\delta z_i)^2/R_{rms}$, due to the error propagation of $\delta z_i=0.05$ nm (scanner resolution). As shown in Fig. 4(b), with increasing film thickness the surface becomes rougher. The relation between R_{rms} and t follows a power law of the form $R_{rms}-t^b$. With linear regression we find $b=0.60\pm0.12$.

The power-law increase of surface roughness is one of the most interesting observations in the thin film growth and has attracted a lot of experimental and theoretical attention

TABLE I. Summary of surface parameters obtained from the analysis of AFM measurements for nanocrystalline Ni/Pt multilayers grown on various substrates and with various thicknesses, as indicated. The maximum error bar in the determination of the mean grain size for both methods (XRD and AFM) is of about ±10%.

Substrate	n	m	Thickness t (nm)	Mean grain size XRD-FWHM D_G (nm)	Mean grain size AFM D_G (nm)	Standard deviation AFM σ (nm)	Roughness AFM R_{rms} (nm)
Glass	10	11	206	35.1	32.01	0.2536	1.014
Glass	15	4	138	30.2	28.80	0.1031	0.764
Glass	2	11.5	108	27.8	24.53	0.1467	0.756
Glass	5	5	85	21.2	21.65	0.1466	0.568
Silicon	5	5	85	22.6	22.13	0.1778	0.435
Kapton	5	5	85	17.7	19.36	0.2384	0.836

the last two decades. As a characteristic example, we refer to the studies of homoepitaxy and heteroepitaxy of single-crystalline films grown by molecular beam epitaxy, where an exponent $b=0.25$ is found for processes dominated by kinetic roughening.[20–22] In cases of polycrystalline/columnar growth and for a proper scale of analysis much larger than the diameter of grains, the predominant roughness source is not any more the roughness within each crystallite but the grain-boundary roughness. In that case b may take much larger values, close to 0.45.[23] Our experimentally determined value of b agrees fairly well with that value. However, the slightly larger value of it could be attributed to two factors, which have been shown to result in large b values: (i) random effects during the deposition process[24] (indeed, a value of $b_1=0.71\pm0.12$ was recently reported by Salvadori *et al.* for Pt thin films prepared, however, by the more energetic metal plasma ion deposition[24]) or (ii) residual strains, which are frequently encountered during thin film growth.[25] We believe that the second factor is more appropriate for our samples, since it is known that Ni/Pt multilayers have a residual strain of about 1%.[26] It is also worth mentioning that values of b, in the range of 0.3–0.8, have also been predicted via modeling of polycrystalline thin film growth considering various growth parameters, see, e.g., Refs. 27 and 28.

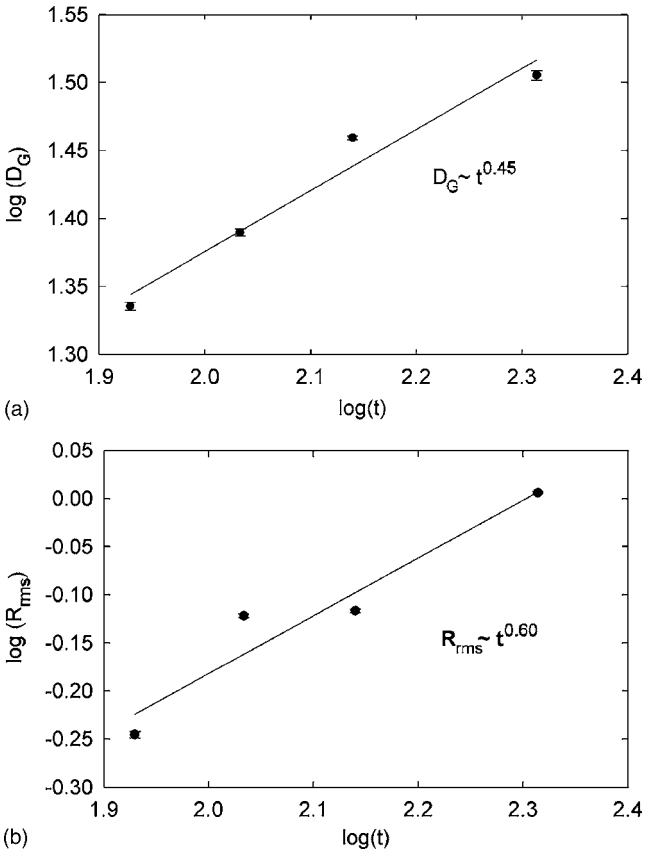

FIG. 4. (a) Variation of the mean grain size with film thickness, for the four samples grown on glass, using the values given in Table I. (b) Variation of average root-mean-square roughness for the four samples grown on glass, with film thickness, using values given in Table I.

In Fig. 5, left column, one may see three-dimensional (3D) AFM images recorded on the surface of three Ni/Pt multilayers with the same thickness and $m=n=5$, grown on silicon (a_1), glass (b_1), and Kapton (c_1). In the right column of Fig. 5, they are shown the corresponding 3D AFM images from the bare substrates of silicon (a_2), glass (b_2), and Kapton (c_2). It is obvious that the sample surface roughness depends on the bare substrate roughness. The sample on Kapton shows the largest mean square roughness $R_{rms}=0.836$ nm, on glass 0.568 nm, and on silicon 0.435 nm. The corresponding values R_{rms} for the substrates are 0.788, 0.147, and 0.082 nm, respectively, see Table II. Therefore, it is meaningful to do comparisons of the roughness as a function of the total thickness only for multilayers grown on the same substrate. The silicon and glass substrates turn out to be almost ideal for such studies due to their very small roughness at the level of 1–2 atomic planes, only.

For the Ni/Pt multilayers grown at 200 °C, it was shown that the surface grains are actually the top view of columns, since those samples presented a well-defined columnar morphology starting directly over the Pt buffer layer.[2] Moreover, it was shown the coexistence of smaller and larger grains in the diameter range 30–250 nm.[2] The latter observation may be confirmed with the help of a new AFM image presented in Fig. 6, for a $Ni_{7.5}/Pt_{4.5}$ multilayer of thickness $t=205$ nm grown at 200 °C on silicon. Now, in order to investigate the shape of the crystallites for the series of samples grown at 40 °C, we have performed TEM investigation on a Ni/Pt multilayer grown on Si(111). The XTEM micrograph of Fig. 7(a) shows the architecture of the multilayer structure just above the Pt buffer layer, revealing the coexistence of spherical and columnar narrow-shaped crystallites, with the latter ones oriented roughly along the growth direction. Across the crystallites and parallel to the surface of the substrate, a wavy layered structure is observed due to the multilayer

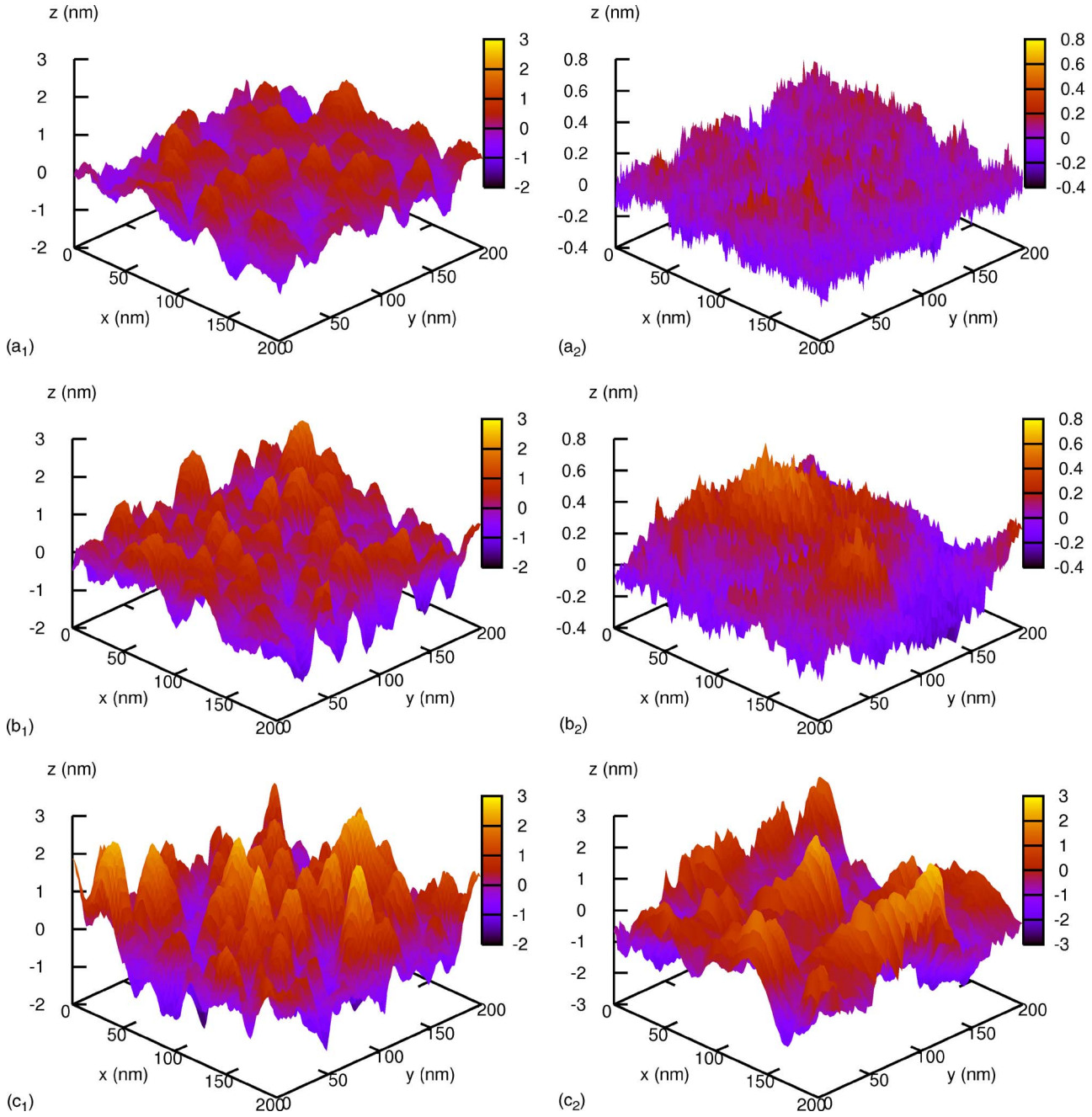

FIG. 5. (Color online) 200×200 nm^2 3D AFM images for three Ni_5/Pt_5 multilayers with the same thickness, grown on (a_1) silicon, (b_1) glass, and (c_1) Kapton and the corresponding substrates (a_2) silicon, (b_2) glass, and (c_2) Kapton.

stacking. The corresponding selected area electron diffraction (SAED) pattern is depicted in Fig. 7(b). Rings of distinct reflections evidence a polycrystalline structure of the multilayer with randomly oriented crystallites, which applies mainly to the independent spherical ones. The arc-shaped intensity of accumulated reflections around the growth direction suggests that columnar grains present a preferred growth orientation along the $[11\bar{1}]$ crystallographic direction of Si [corresponding SAED pattern of Si—Fig. 7(c)] and they are misoriented within ±15° around it. Having as a reference the

TABLE II. Summary of roughness parameters for a set of three Ni_5/Pt_5 multilayers with same total thickness $t=85$ nm, grown on silicon, glass, and Kapton. The substrate roughness parameters are also shown. The maximum error bars are of the order of 10%.

	Grown on silicon	Grown on glass	Grown on Kapton	Silicon	Glass	Kapton
R_{p-p} (nm)	2.602	4.242	4.950	0.714	1.137	4.922
R_a	0.353	0.462	0.667	0.072	0.130	0.620
R_{rms}	0.435	0.568	0.836	0.090	0.163	0.788

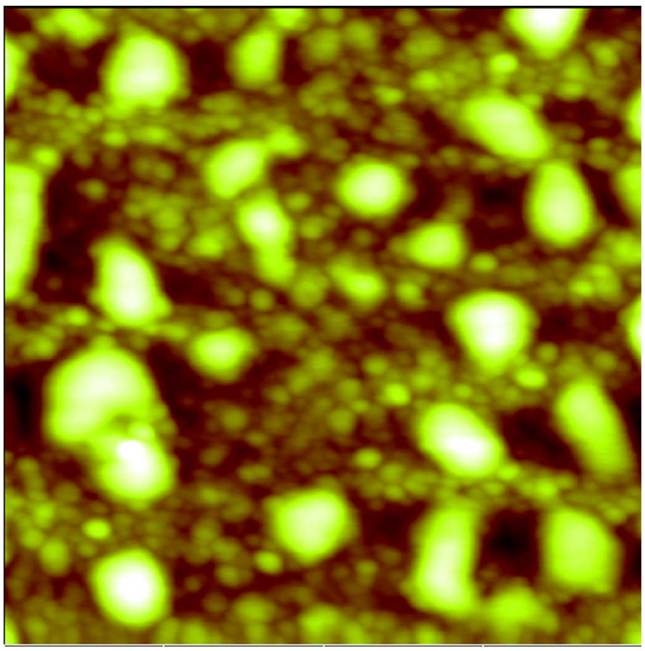

FIG. 6. (Color online) AFM image recorded on the surface of a $Ni_{7.5}/Pt_{4.5}$ multilayer of thickness $t=205$ nm grown at 200 °C on silicon. A bimodal growth mode is clearly observed. The size of the images is 1×1 μm^2.

d-spacing values of the SAED pattern of Si that are well-known, $d_1=0.214\pm0.001$ nm and $d_2=0.185\pm0.001$ nm *d*-spacing values of the inner two polycrystalline rings were measured from the SAED pattern of Fig. 7(b), which do not match either Pt or Ni *d*-spacing bulk values, whereas their relative ratio ($d_1/d_2=1.156$) indicates a cubic lattice. Since the fairly large field of view of the SAED comprises a substantial number of bilayers, the *d* spacing of the polycrystalline rings can be explained in terms of an average fcc lattice originating from a combination of the Pt and Ni fcc lattices. In a first approximation, *d* spacing of low-index planes of the average lattice can be calculated from the expression $\bar{d}_{hkl}=\Lambda/(N_{Ni}+N_{Pt})$, where Λ is the bilayer thickness and N_{Ni}, N_{Pt} are the number of atomic *hkl* planes per bilayer of Ni and Pt, respectively.[29] From high-resolution TEM micrographs, we measure $\Lambda=1.45$ nm, divided in approximately 0.68 nm for Pt and 0.77 nm for Ni, which corresponds to a succession of an average $Ni_{3.8}/Pt_3$ planes per bilayer along the growth direction. Therefore, for $d_{111}(Pt)=0.2265$ nm and $d_{111}(Ni)=0.20345$ nm (bulk values), the $\bar{d}_{111}$ of the average lattice is $\bar{d}_{111}=0.2136$ nm. Moreover, for $d_{200}(Pt)=0.1962$ nm, $d_{200}(Ni)=0.17619$ nm (bulk values), the $\bar{d}_{200}$ of the average lattice is $\bar{d}_{200}=0.185$ nm. These calculated values show a remarkable resemblance to the experimentally measured d_1 and d_2 values, hence, strengthening the hypothesis of the multilayer adopting an average fcc cubic lattice. The lattice constant of the average fcc lattice is $\bar{a}=0.371$ nm compared to the $a=0.39231$ nm of Pt and to the $a=0.35238$ nm of Ni, as expected by the application of Vegard's law.[11] For this sample, since both, *m* and *n* values, are very small, interdiffusion between adjacent layers of Ni and Pt is considerable [Fig. 7(a), inset], in agreement with Ref. 7.

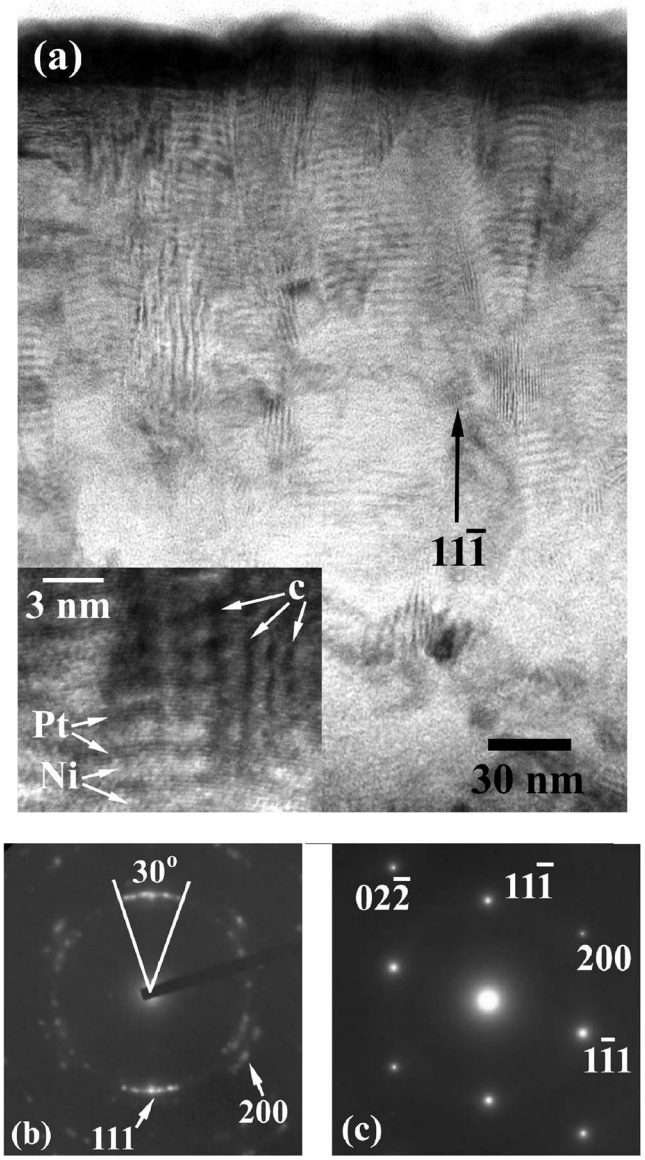

FIG. 7. (a) TEM micrograph showing the crystal structure of the modulated multilayer, above the buffer layer, and the coexistence of spherical and columnar grains. Interdiffusion between adjacent Pt and Ni layers is important due to the extremely small values $n=3.8$ and $m=3.0$ along the growth direction (inset). The average lattice spacing in both Pt, Ni layers remains constant suggesting the adoption of an average lattice by the multilayer. Columnar grains are denoted with *c*. (b) Corresponding SAED pattern of the multilayer illustrating its polycrystalline nature. The relative ratio $d_1/d_2=1.156$ of the two inner rings indicate a fcc cubic lattice, whereas arc-shaped reflections show a preferential growth orientation of the columnar grains within ±15° around the growth direction. (c) Corresponding SAED pattern of the Si substrate depicting the [11$\bar{1}$] growth direction of the multilayer.

The different growth habits of samples evaporated at 200 and 40 °C may be understood as follows: Hentzel *et al.* have presented a study of growth of mainly single element and some alloyed metallic thin films.[30] They have shown that the mean grain size strongly depends on the ratio of T_m/T_S. For relatively large values of this ratio, i.e., lower substrate temperatures, one observes smaller grains with a narrower size distribution, such as ours grown at 40 °C. On the contrary, for relatively small values of the T_m/T_S ratio, a larger distribution of the grain size and very large grains could be

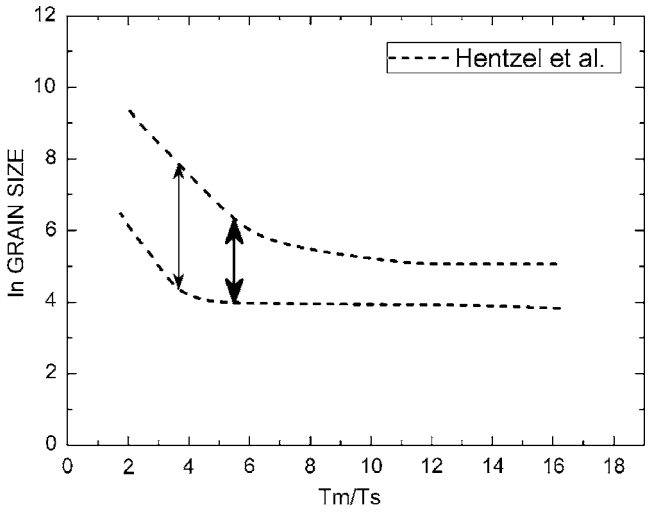

FIG. 8. The dashed lines represent the limits for the ln GRAIN for many metallic thin film systems as a function of the T_m/T_S ratio (see Ref. 30), while the arrows indicate the expected ranges of grain sizes for our Ni/Pt multilayer series grown at 40 °C (thick) and 200 °C (thin arrow).

present. In Fig. 8 the results of Hentzel *et al.* are plotted by the two dashed lines. The upper (lower) represents the upper (lower) limit for the grain size as a function of T_m/T_S. Therefore, we attempted to see whether metallic multilayers could fit to the construction of Hentzel *et al.*, for the first time, to our knowledge. For an estimate of the T_m of our multilayers we have used the binary alloy phase diagrams of the NiPt system,[31] considering the average concentration of the multilayer to be the same as that of an alloy. Then, for the lower substrate temperature value we have $T_m/T_S \approx 5.5$, while for the higher substrate temperature value we have $T_m/T_S \approx 3.6$. In Fig. 8 the thick (thin) arrow is used to predict the minimum and maximum grain size expected for multilayers grown at the lower (higher) substrate temperature. The grain size limits are estimated to be 5 and 50 nm for the lower and 10 and 250 nm for the higher temperature, in fair agreement with our experimental results.

One may incorporate the aforementioned results in the framework of structural zone models.[11,30] To compare to existing literature it is more convenient to consider this time the inverse ratio T_S/T_m. The T_S/T_m ratio for both evaporation temperatures suggests that our samples belong to the structural zone *T*.[10,30] The 40 °C series, with a $T_S/T_m=0.18$ is closer to zone I, where predominantly the film is formed via the process of continuing renucleation of grains during deposition. As a result, a large fraction of crystallites has spherical shape and the few columns have not grown much in size due to lower kinetics of the adatoms. Our AFM images resemble to a large extent the schematics in terms of the structural zone model *T* at $T_S/T_m=0.18$.[30] The 200 °C series samples have a $T_S/T_m=0.28$. While the structural zone model *T* is again the appropriate to describe the crystal growth, this time we are much closer to zone II.[30] Zone II structures are columnar and the dominant mechanism is growth, rather than nucleation. Therefore, a bimodal growth mode (coexistence of large columns and fewer in terms of volume small grains) becomes obvious, as also our AFM image of Fig. 6 reveals. Consequently, our AFM and XTEM observations can be well-understood within the framework of structural zone models.

C. Resistance against aging effects

Finally, we tune to the matter of aging in metallic magnetic multilayers. This matter is rarely addressed, however, it is of great importance for the use of magnetic multilayers as magnetic recording media. A degradation or loss of the interface quality is expected to result in degradation of magnetic properties, like, e.g., the perpendicular magnetic anisotropy, which are important for applications. This will happen because perpendicular magnetic anisotropy is a result of interface anisotropy and/or of the strain at interfaces. Since multilayers are highly metastable structures,[11] increase of temperature and/or age could drive these systems to their thermodynamical stable state; this is the formation of solid solutions according to the binary alloy phase diagram of the NiPt system.[31] In order to check the stability of the Ni/Pt system we have taken one of the most important samples, the $Ni_8/Pt_{1.7}$ multilayer appearing in Ref. 2. This sample shows perpendicular magnetic anisotropy,[2] enhanced magneto-optic response,[2,4] and possesses very thin layers, therefore it could be very sensitive to aging effects. We have stored this sample for 12 years after its growth in an atmospheric air environment at room temperature, such as the one that a computer hard disk is expected to be stored. Of course, in applications such as the thermomagnetic recording, under operational conditions, the disk is warmed up at temperatures close to the Curie temperature. A benefit of the Ni/Pt multilayer system is the relatively low Curie temperatures.[2] Therefore, one would not expect operational temperatures larger than 200 °C, which are safe enough to prohibit interdiffusion as previous studies have shown.[2,6,7] We have performed an XRD scan of this sample 12 years after its preparation and this scan is shown in Fig. 9 ("new") together with the XRD scan recorded just after its preparation 12 years ago ("old"). The multilayer maintains all its multilayer diffractions. It is amazing the fact that it still presents a third order diffraction much above $2\theta=10$ °C, as a high quality sample is expected and its XRD pattern remains the same as when it was prepared. Moreover, we have recorded a hysteresis loop with the magnetic field applied along the film normal (see Fig. 10), which according to Ref. 2 should be the easy magnetization axis for the sample. The hysteresis loop is practically identical to the one appearing in Ref. 2 for the $Ni_8/Pt_{1.7}$ multilayer. Our results show that both, layering and useful magnetic properties of Ni/Pt multilayers remain unchanged for a period of at least 12 years. This resistance against aging could be understood by the existence of a high energy barrier between the two metallic layers, which prohibits significant interdiffusion for the Ni/Pt system. In conclusion, Ni/Pt multilayers can be safely used as hard disks in the magnetic/magneto-optic recording industry.

IV. SUMMARY

A comparative study of N/Pt multilayers grown at different substrate temperatures, namely 40 and 200 °C, is pre-

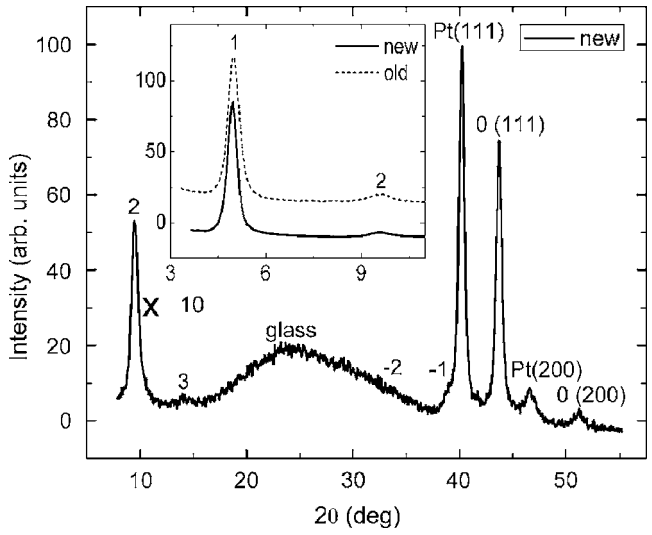

FIG. 9. X-ray diffraction pattern recorded for a $Ni_8/Pt_{1.7}$ multilayer grown at 200 °C on glass. The multilayer is 12 years old. Despite the extremely thin Pt layers the multilayer structure maintains, as can be mainly seen by the presence of three small-angle multilayer diffractions. In the inset one may see the small angle XRD pattern recorded on the as-prepared sample (dashed line) and 12 years after. The patterns in the inset have been vertically shifted for better presentation.

sented. The multilayer stacking is slightly worse for samples grown at the lower temperature due to some interface roughness. The main source of roughness, however, originates from the grain boundaries and presents a power law increase with the samples' thickness. Samples grown at the lower temperature show a homogeneous grain-size distribution with mean grain size in the order of 20–30 nm, while the ones grown at the higher temperature show a broader grain-size distribution. Both samples grown at 40 and 200 °C can be classified at the two edges of the same transitional structural zone *T*. Finally, Ni/Pt multilayers show high resistance against aging, i.e., they could be successfully employed in the magnetic recording industry for the preparation of long-life hard disks.

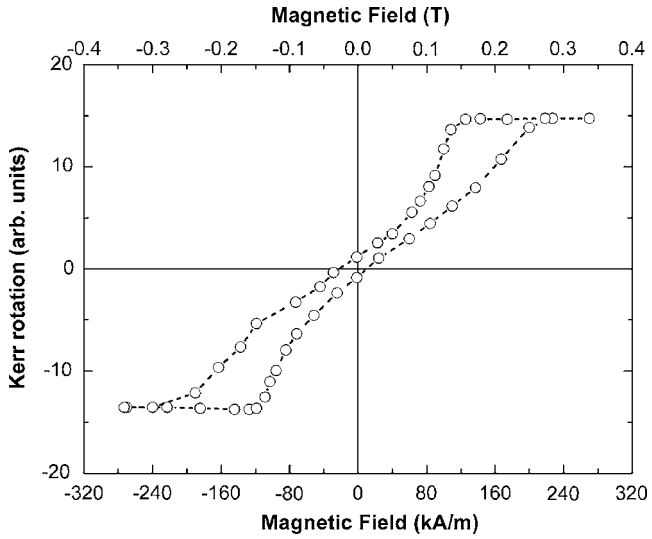

FIG. 10. Polar Kerr rotation hysteresis loop for a $Ni_8/Pt_{1.7}$ multilayer grown at 200 °C on glass. The multilayer is 12 years old.

ACKNOWLEDGMENTS

Work was supported by the Greek Secretariat for Research and Technology (GSRT), Project PENED2003 "Self-assembled networks of magnetic nanoparticles for applications of permanent magnets, sensors and magnetic recording media." One of the author (E.Th.P.) is grateful to the Collaborative Research Center 658 for financial support and the Freie Universität Berlin for the excellent hospitality.

[1] R. Krishnan, H. Lassri, M. Porte, M. Tessier, and P. Renaudin, Appl. Phys. Lett. **59**, 3649 (1991).
[2] M. Angelakeris, P. Poulopoulos, N. Vouroutzis, M. Nyvlt, V. Prosser, S. Visnovsky, R. Krishnan, and N. K. Flevaris, J. Appl. Phys. **82**, 5640 (1997).
[3] S.-C. Shin, G. Srinivas, Y.-S. Kim, and M.-G. Kim, Appl. Phys. Lett. **73**, 393 (1998).
[4] E. Th. Papaioannou, M. Angelakeris, N. K. Flevaris, P. Fumagalli, Ch. Mueller, A. Troupis, A. Spanou, V. Karoutsos, P. Poulopoulos, V. Kapaklis, and C. Politis, J. Appl. Phys. **101**, 023913 (2007).
[5] F. Wilhelm, P. Poulopoulos, P. Srivastava, H. Wende, M. Farle, K. Baberschke, M. Angelakeris, N. K. Flevaris, W. Grange, J.-P. Kappler, G. Ghiringhelli, and N. B. Brookes, Phys. Rev. B **61**, 8647 (2000).
[6] F. Wilhelm, P. Poulopoulos, G. Ceballos, H. Wende, K. Baberschke, P. Srivastava, D. Benea, H. Ebert, M. Angelakeris, N. K. Flevaris, D. Niarchos, A. Rogalev, and N. B. Brookes, Phys. Rev. Lett. **85**, 413 (2000).
[7] P. Poulopoulos, F. Wilhelm, H. Wende, K. Baberschke, D. Benea, H. Ebert, M. Angelakeris, N. K. Flevaris, A. Rogalev, and N. B. Brookes, J. Appl. Phys. **89**, 3874 (2001).
[8] R. Krishnan, H. Lassri, S. Prasad, M. Porte, and M. Tessier, J. Appl. Phys. **73**, 6433 (1993).
[9] S. Sun, C. B. Murray, D. Weller, L. Folks, and A. Moser, Science **287**, 1989 (2000).
[10] M. Ohring, *Materials Science of Thin Films*, 2nd ed. (Academic, San Diego, 2002).
[11] B. Y. Jin and J. B. Ketterson, Adv. Phys. **38**, 189 (1989), and references therein.
[12] M. A. Escobar, L. F. Magana, and R. Valenzuela, J. Appl. Phys. **57**, 2142 (1985).
[13] A. Guinier, *X-Ray Diffraction in Crystals, Imperfect Crystals and Amorphous Bodies* (Dover, New York, 1963).
[14] V. Kapaklis, P. Poulopoulos, V. Karoutsos, Th. Manouras, and C. Politis, Thin Solid Films **510**, 138 (2006).
[15] K. Cai, M. Müller, J. Bossert, A. Rechtenbach, and K. D. Jandt, Appl. Surf. Sci. **250**, 252 (2005).
[16] J. R. Shi, S. P. Lau, Z. Sun, X. Shi, B. K. Tay, and H. S. Tan, Surf. Coat. Technol. **138**, 250 (2001).
[17] A. Amaral, P. Brogueira, C. N. de Carvalho, and G. Lavareda, Surf. Coat. Technol. **125**, 151 (2000).
[18] M. Maqbool and T. Khan, Int. J. Mod. Phys. B **20**, 217 (2006).
[19] L. L. Melo, M. C. Salvadori, and M. Cattani, Surf. Rev. Lett. **10**, 903 (2003).
[20] M. Siegert and M. Pliscke, Phys. Rev. Lett. **73**, 1517 (1994).
[21] J.-K. Zuo and J. F. Wendelken, Phys. Rev. Lett. **78**, 2791 (1997).
[22] P. Poulopoulos, J. Lindner, M. Farle, and K. Baberschke, Surf. Sci. **437**, 277 (1999).
[23] L. Vazquez, R. C. Salvarezza, P. Herrasti, P. Ocon, J. M. Vara, and A. J. Arvia, Surf. Sci. **345**, 17 (1996).
[24] M. C. Salvadori, L. L. Melo, M. Cattani, O. R. Monteiro, and I. G. Brown, Surf. Rev. Lett. **10**, 1 (2003).
[25] T.-B. Hur, Y.-H. Hwang, H.-K. Kim, and H.-L. Park, J. Appl. Phys. **96**, 1740 (2004).
[26] W. Steiger, A. Michel, V. Pierron-Bohnes, N. Hermann, and M. Cadeville, J. Mater. Res. **12**, 161 (1997).
[27] D. J. Srolovitz, J. Vac. Sci. Technol. A **4**, 2925 (1986).
[28] J. Zhang and J. B. Adams, Comput. Mater. Sci. **31**, 317 (2004).
[29] Th. Kehagias, Ph. Komninou, C. Christides, G. Nouet, S. Stavroyiannis, and Th. Karakostas, J. Cryst. Growth **208**, 401 (2000).
[30] H. T. G. Hentzell, C. R. M. Grovenor, and D. A. Smith, J. Vac. Sci. Technol. A **2**, 218 (1984).
[31] T. B. Massalski, *Binary Alloy Phase Diagrams* (ASM, Metals Park, OH, 1986), Vol. 1, p. 29.